separations

MDPI

Article

Photocatalytic Degradation of Ciprofloxacin: A Combined Experimental and Theoretical Study Using Curcumin and Hydrogen Peroxide

Flórida L. P. de Paiva [1], Maria Vivian C. Silva [1], Ana Lara F. Mendonça [1], Cristiane S. Araújo [1], Lóide O. Sallum [2], Antonio S. N. de Aguiar [1], Alessandra R. Lima [3], Hamilton B. Napolitano [1,4], Mário J. F. Calvete [5] and Lucas D. Dias [1,*]

[1] Laboratório de Novos Materiais, Universidade Evangélica de Goiás, Anapolis 75083-515, GO, Brazil; floridalorena@gmail.com (F.L.P.d.P.); m.vcsilva@hotmail.com (M.V.C.S.); analaraferreira060322@gmail.com (A.L.F.M.); cristiane.araujo@unievangelica.edu.br (C.S.A.); toninho.quimica@gmail.com (A.S.N.d.A.); hbnapolitano@gmail.com (H.B.N.)
[2] Laboratório de Ciências Farmacêuticas, Universidade Evangélica de Goiás, Anapolis 75083-515, GO, Brazil; loide.sallum@gmail.com
[3] Instituto de Física de São Carlos, Laboratório de Biofotônica Ambiental, Universidade de São Paulo, São Carlos 13560-970, SP, Brazil; ramos.alessandra.09@gmail.com
[4] Grupo de Química Teórica e Estrutural de Anápolis, Universidade Estadual de Goiás, Anapolis 75083-515, GO, Brazil
[5] Centro de Química de Coimbra, Departamento de Química, Universidade de Coimbra, Rua Larga, 3004-535 Coimbra, Portugal; mcalvete@qui.uc.pt
* Correspondence: lucasdanillodias@gmail.com

Abstract: Contamination of soil, water, and wastewater by pharmaceuticals, including antibiotics, is a global health problem. This work evaluated the use of a natural compound, curcumin (CUR), as a homogeneous photocatalyst, together with hydrogen peroxide (H_2O_2) as a benign oxidant, to promote the photodegradation of ciprofloxacin (CIP). Furthermore, we carried out theoretical calculations using density functional theory (DFT) to assess the chemical reactivity of ciprofloxacin. In addition, the intermolecular interaction patterns of two crystalline polymorphs of the antibiotic drug were analyzed through Hirshfeld surfaces. Finally, calculations using the TD-DFT formalism were carried out to understand the effects on the CIP molecule caused by the simultaneous presence of the CUR molecule and ultraviolet-visible light (UV-Vis). A photooxidative effect was observed in the presence of the CUR photocatalyst (CIP + CUR (1:0.5)), resulting in a degradation of CIP of up to 24.4%. However, increasing the concentration of the CUR photocatalyst (ciprofloxacin + curcumin (1:1)) decreased the photodegradation of CIP, which may be caused by competition between the CIP molecule and CUR for ROS generated in situ. Additionally, the calculation results showed that the electronic excitations caused by the associated CIP + CUR structures affect the CIP molecule, resulting in the effects observed experimentally. The results show that CUR, when applied as a photosensitizing catalyst, presents synergistic potential with H_2O_2 in the photocatalytic degradation of ciprofloxacin. This photocatalytic process can be applied to the environmental remediation of pharmaceutical micropollutants, a subject of ongoing studies.

Keywords: photodegradation; environment; antibiotic; ciprofloxacin; curcumin; hydrogen peroxide; molecular modeling

check for updates

Citation: de Paiva, F.L.P.; Silva, M.V.C.; Mendonça, A.L.F.; Araújo, C.S.; Sallum, L.O.; de Aguiar, A.S.N.; Lima, A.R.; Napolitano, H.B.; Calvete, M.J.F.; Dias, L.D. Photocatalytic Degradation of Ciprofloxacin: A Combined Experimental and Theoretical Study Using Curcumin and Hydrogen Peroxide. *Separations* **2024**, *11*, 260. https://doi.org/10.3390/separations11090260

Academic Editor: Grzegorz Boczkaj

Received: 1 August 2024
Revised: 29 August 2024
Accepted: 29 August 2024
Published: 2 September 2024

Copyright: © 2024 by the authors. Licensee MDPI, Basel, Switzerland. This article is an open access article distributed under the terms and conditions of the Creative Commons Attribution (CC BY) license (https://creativecommons.org/licenses/by/4.0/).

1. Introduction

Antibiotics are a class of pharmaceuticals that are widely applied to support global health by treating infectious diseases in humans and animals [1,2]. In 2022, the European Centre for Disease Prevention and Control reported an antibiotic consumption of 19.4 defined daily doses (DDD) per 1000 inhabitants per day [3]. This large consumption in

different sectors results in the contamination of soil and water by non-used antibiotics, resulting in the development of resistant bacteria [4,5]. In this regard, antimicrobial resistance is considered a major global public health issue, being responsible for nearly 5 million deaths in 2019 and producing US$ 1 trillion in additional healthcare costs by 2050 [6]. Moreover, Sustainable Development Goal 3 reports the need for "access to safe, effective, quality, and affordable essential medicines and vaccines for all". This worldwide goal addresses a wide range of health challenges and improves health systems globally [7,8].

Ongoing research aims to decrease the use of antibiotics in society through awareness and/or the development of technologies capable of removing or degrading antibiotics in soil, water, or wastewater [9–14]. In this regard, catalytic processes using adequate light sources are largely applied, aiming to transform antibiotic molecules into non-toxic degradation products through homogeneous, heterogeneous, and enzymatic catalysis [15–17]. Among these, the use of hybrid metal-based photocatalysts [18–22] and green oxidants (molecular oxygen, O_2, and/or hydrogen peroxide, H_2O_2) has been showing promising results with potential applications in large-scale industrial processes [23,24]. Other types of photocatalysts, based on organic materials such as the biomimetic porphyrin macrocycles and their metal complexes, have also been recently used as valid alternative photosensitizing catalysts for pollutant degradation (including antibiotics) [24–27]. The utilization of natural photosensitizers represents a sustainable pathway for many applications, including curcumin [28–30], which is widely recognized for its potential in photodynamic therapy due to its non-toxic nature, availability, and effectiveness in generating reactive oxygen species under light exposure [28].

This work aimed to evaluate the photodegradation of the second-generation fluoroquinolone ciprofloxacin in an aqueous medium, using curcumin (CUR) as a non-toxic homogeneous catalyst and H_2O_2 as an oxidant. This study was supported by experimental tests using different catalyst concentrations in the presence and absence of oxidants. Understanding the patterns of intermolecular interactions of ciprofloxacin hydrochloride polymorphs and the electronic structure of the drug and its electronic transitions can provide relevant information during the photocatalytic processes in wastewater. Therefore, calculations supported by time-dependent density functional theory (TD-DFT) were carried out to obtain such information.

2. Materials and Methods

2.1. Hirshfeld Surface Analysis

The supramolecular arrangements of two polymorphs of ciprofloxacin hydrochloride (CIP) were analyzed. Their structures were obtained from the Cambridge Crystallography Data Center (CCDC), with the codes 1982374 (polymorph I) and 1982376 (polymorph II) [28]. The intermolecular interaction patterns of these polymorphs were carried out by the Mercury program [31], and the intermolecular contacts, as well as the crystal packing of the polymorphs, were analyzed through the Hirshfeld surfaces (HS) [32] with the aid of the PLATON [33] and CrystalExplorer 21.5 programs [34]. The HS was calculated based on the distances between the inner core (d_i) and the outer core (d_e) of the molecule [35], respectively. The normalized contact distances (d_{norm}) were used to identify the most important contacts between molecules in the crystals of the polymorphs, and the shape indices, a function that depends on the HS curvature, were analyzed, providing information about the hydrophobic interactions in the molecule [36]. Finally, the 2D fingerprint plots were used to calculate the quantities and frequencies of the intermolecular contacts existing in the molecule.

2.2. Molecular Modeling

The calculations were carried out using the DFT [37,38] method, which was implemented in the Gaussian 16 software package [39]. To determine the most suitable level of theory for the studied molecular systems, it was used the M06-2X [40], B3LYP [41,42], X3LYP [43], and ωB97XD functionals and compared their geometric parameters to those

obtained experimentally by X-ray diffraction. Frequency calculations were carried out to ensure that the wave function reached the lowest energy state. With the molecule completely optimized, the isosurfaces and the energies of the frontier molecular orbitals (FMO) [44]—the highest occupied molecular orbital (HOMO) and the lowest unoccupied molecular orbital (LUMO)—and molecular electrostatic potential (MEP) [45] were extracted using the GaussView 6.0 program [46]. From the FMO energies, the chemical reactivity descriptors of the CIP molecule were predicted and compared to those of the neutral ciprofloxacin (CIPneutral) molecule. The descriptors analyzed were chemical hardness [47,48], chemical potential [47], and the global electrophilicity index [49]. Furthermore, through the Fukui function [50,51], it was possible to predict the reactivity sites, like nucleophilic, electrophilic, and radical attacks.

To understand the photoprotective process of CUR over CIP, theoretical calculations of the excited states of the CIP, CUR, and CIP + CUR molecules were carried out. Based on the MEP of the CIP and CUR molecules, the associated structures were constructed in such a way that the regions of high charge density of one molecule were placed in contact with the regions of low charge density of the other and vice versa, forming the structures represented in Figure S6 (Supplementary Material). The structures were optimized in the presence of an implicit solvent (water) using the SMD continuum solvation model [52]. From the completely optimized structures, the calculations of the excited states were carried out using the TD-DFT [53] method using the CAM-B3LYP/6-311++G(d,p) level of theory.

2.3. Photodegradation Process of Ciprofloxacin Using Curcumin as Catalyst

An aqueous stock solution of CIP at 9.43 mM was prepared (100 mL, pH = 7). Then, H_2O_2 (final concentration: 3.5%) and/or CUR as photocatalyst (86.8 mg; 9.434 mmol or 43.4 mg; 4.717 mmol) were added (when applicable) resulting in the following groups:

G1: 9.43 mM ciprofloxacin
G2: 9.43 mM ciprofloxacin + 1.16 M hydrogen peroxide
G3: 9.43 mM ciprofloxacin + 4.71 mM curcumin
G4: 9.43 mM ciprofloxacin + 9.43 mM curcumin
G5: 9.43 mM ciprofloxacin + 1.16 M hydrogen peroxide + 4.71 mM curcumin
G6: 9.43 mM ciprofloxacin + 1.16 M hydrogen peroxide + 9.43 mM curcumin

The final solutions (**G1**–**G6**) were submitted to irradiation using a fluorescent lamp (6.4×10^{-4} W/cm^2) for 72 h. For analytical analysis, an aliquot (5 mL) was taken from the reaction media at 0, 24, 48, and 72 h, respectively.

2.4. Chromatographic Analysis of Photodegradation Products

The aliquots obtained from the reaction media were filtrated using a Millex-FH (MilliporeSigma, Burlington, MA, USA) 0.45 µm and submitted to chromatographic analysis using a Shimadzu LC-2050 and the following conditions: C18 column (4.6 mm × 150 mm × 5 µm), wavelength at 280 nm, mobile phase (2% acetic acid solution: acetonitrile) (84:16), flow rate at 1.0 mL/min, injection volume of 10 µL, and run time of 14 min. The chromatograms obtained were analyzed using LabSolutions software (LabSolutions LC 5.92).

3. Results

3.1. Molecular Modeling Analysis

The CIP asymmetric unit for polymorphic forms I (Figure 1a) and II (Figure 1b) is shown in the ORTEP diagrams. The conformer I crystallizes in the $P2_1/c$ monoclinic space group; on the other hand, the conformer II crystallizes in the Pbca orthorhombic space group, and the crystal data and refinement details for conformers I and II are summarized in Table S1 (Supplementary Material). The root mean square (RMS) value between the CIP polymorphic forms I and II was 0.0173, as shown in the overlay of these conformers I (black) and II (yellow) in Figure 1c. The conformational differences observed on the piperazine ring of the CIP polymorphs indicate that they are conformational polymorphs.

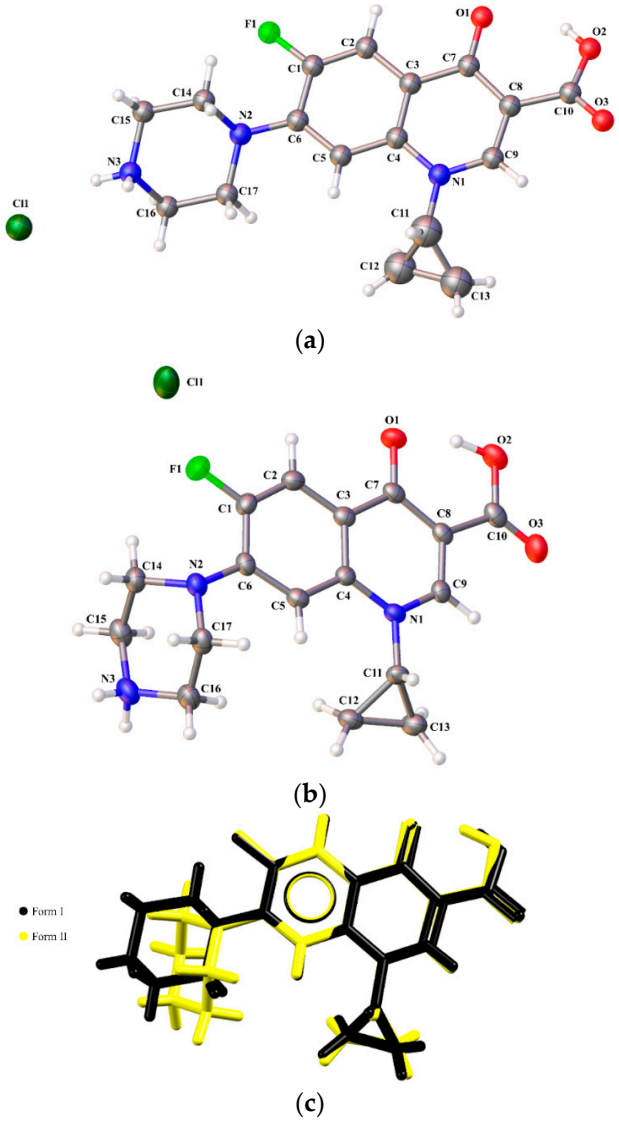

Figure 1. ORTEP representation of the ciprofloxacin hydrochloride (CIP) asymmetric unit for polymorphic (**a**) form I, (**b**) form II with the atom numbering scheme, and (**c**) overlay of forms I (black) and II (yellow). Ellipsoids are drawn at the 50% probability level.

Both CIP polymorphic forms I and II make the classical O_2–$H_2\cdots O_1$ and non-classical C_{14}–$H_{14}\cdots F_1$ intramolecular interactions forming conjugated six-membered rings. We employed HS mapped over d_{norm} (ranging from –0.4326 to 1.7436 Å for form I and –0.5706 to 1.4600 Å for form II) to interpret the most dominant interactions, which are analyzed based on the distances from HS to the nearest atom outside (d_e) and inside (d_i) to the surface, as shown in Figure 2. On the HS d_{norm}, the red dots represent the strong interactions in the crystal packing, as shown in Table 1.

The crystal packing for form I of the CIP corresponds to the chloride anion participating in N_3–$H_{3A}\cdots Cl_1$ and N_3–$H_{3B}\cdots Cl_1$ intermolecular interactions growing in a zig-zag chain along the *b*-axis, which can be described as $C_2^1(4)$ [54]. Also, N_3–$H_{3B}\cdots Cl_1$ forms a ring with C_{17}–$H_{17B}\cdots Cl_1$ intermolecular interaction, which can be described as $R_2^1(6)$, as shown in Figure 2a. The red dots in Figure 3b are related to C_{14}–$H_{14A}\cdots F_1$ and C_{12}–$H_{12B}\cdots O_1$ intermolecular interactions forming a ring around the inversion center, which appears as a two-dimensional (2D) sheet on the crystal supramolecular arrangement, which can be described as $R_2^2(18)$. Finally, non-classical C_{15}–$H_{15B}\cdots O_3$ intermolecular interaction forms a zig-zag chain, which grows along the c-axis and can be described as $C_1^1(12)$, as shown in Figure 2c. The crystal packing for form I of the CIP is formed by the classical

and non-classical intermolecular interactions as well as π···π stacking interactions formed by the centroids Cg1–Cg1 (C_1–C_6) and Cg2–Cg2 (C_3–C_4–N_1–C_9–C_8–C_7), whose distances are 3.67 and 3.72 Å, respectively, which can be shown on shape index HS by red and blue triangles, as shown in Figure 2d.

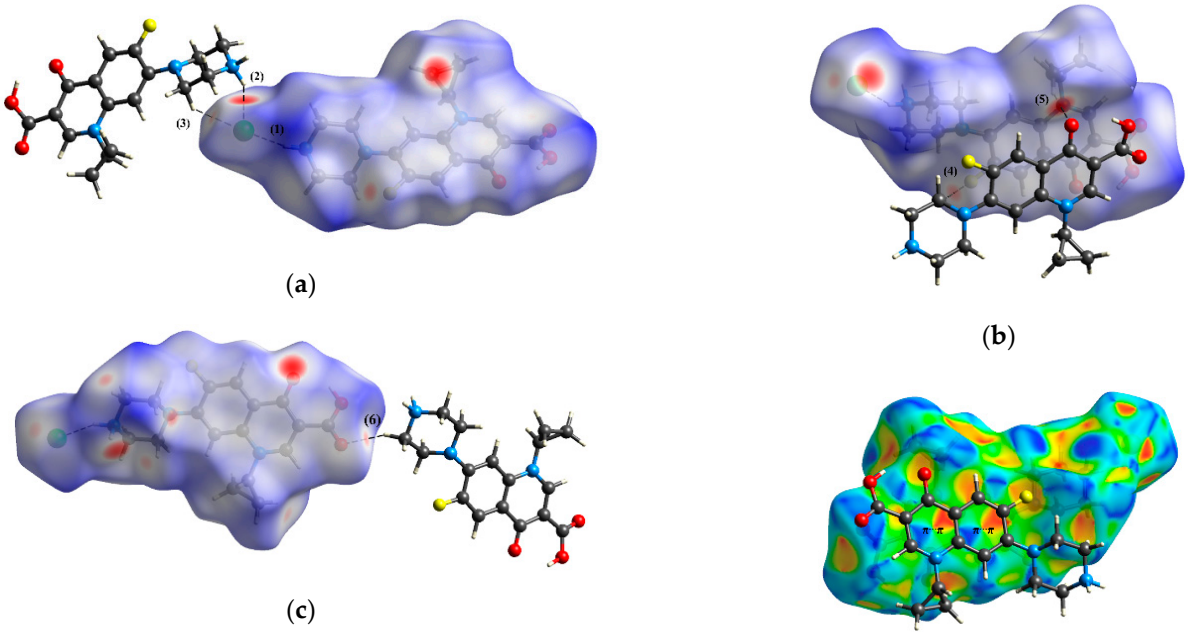

(**1**) N_3–H_{3A}···Cl_1 (**4**) C_{14}–H_{14A}···F_1

(**2**) N_3–H_{3B}···Cl_1 (**5**) C_{12}–H_{12B}···O_1

(**3**) C_{17}–H_{17B}···Cl_1 (**6**) C_{15}–H_{15B}···O_3

Figure 2. The HS d_{norm} showing (**a**) N_3–H_{3A}···Cl_1, N_3–H_{3B}···Cl_1, and C_{17}–H_{17B}···Cl_1; (**b**) C_{14}–H_{14A}···F_1 and C_{12}–H_{12B}···O_1; (**c**) C_{15}–H_{15B}···O_3 intermolecular interactions; and (**d**) π···π stacking found in the crystal packing for form I of the CIP.

Table 1. Hydrogen-bond geometry (Å, °) in the crystal structure of ciprofloxacin hydrochloride's polymorphs.

CIP	D–H···A	D···H	D···A	H···A	D–H···A	Symmetry Code
Form I	N_3–H_{3A}···Cl_1	0.88	2.993	2.17	156.00	½ − x, −½ + y, z
	N_3–H_{3B}···Cl_1	0.88	3.197	2.41	149.00	½ + x, y, ½ − z
	C_{17}–H_{17B}···Cl_1	0.96	3.565	2.78	140.00	½ + x, y, ½ − z
	C_{14}–H_{14A}···F_1	0.96	3.181	2.41	137.00	½ − x, ½ + y, z
	C_{12}–H_{12B}···O_1	0.96	3.069	2.16	158.00	½ − x, −½ + y, z
	C_{15}–H_{15B}···O_3	0.96	3.452	2.55	158.00	½ − x, 1 − y, ½ +z
Form II	N_3–H_{3A}···Cl_1	0.94	3.059	2.13	174.00	2 − x, 1 − y, −z
	N_3–H_{3B}···Cl_1	0.96	3.069	2.11	175.00	x, ½ − y, –½ + z
	C_{12}–H_{12A}···O_1	0.99	3.324	2.47	144.00	x, 3/2 − y, −½ + z
	C_{14}–H_{14B}···O_3	0.99	2.868	2.19	158.50	1 + x, y, z

The 2D fingerprint plot of the CIP is shown in Figure 4. The 2D fingerprint plots (d_i vs. d_e) identify and quantify the intermolecular interactions in the solid-state arrangement [32]. These H···H contacts make up 36.9% and 33.3% of the HS for forms I and II of the CIP, respectively. The O···H/H···O contacts are the second largest contributions for form I of the CIP with 21.9% of the HS, and it is shown as the spikes at the bottom of the 2D fingerprint plot. The red spots Cl···H/H···Cl contacts, which are the second highest

contributions with 22.4% for form II of the HS of CIP, are shown as the spikes at the bottom of the 2D fingerprint plot. Finally, C···C contacts represent 8.7% and 7.9% of the HS of CIP for forms I and II, respectively.

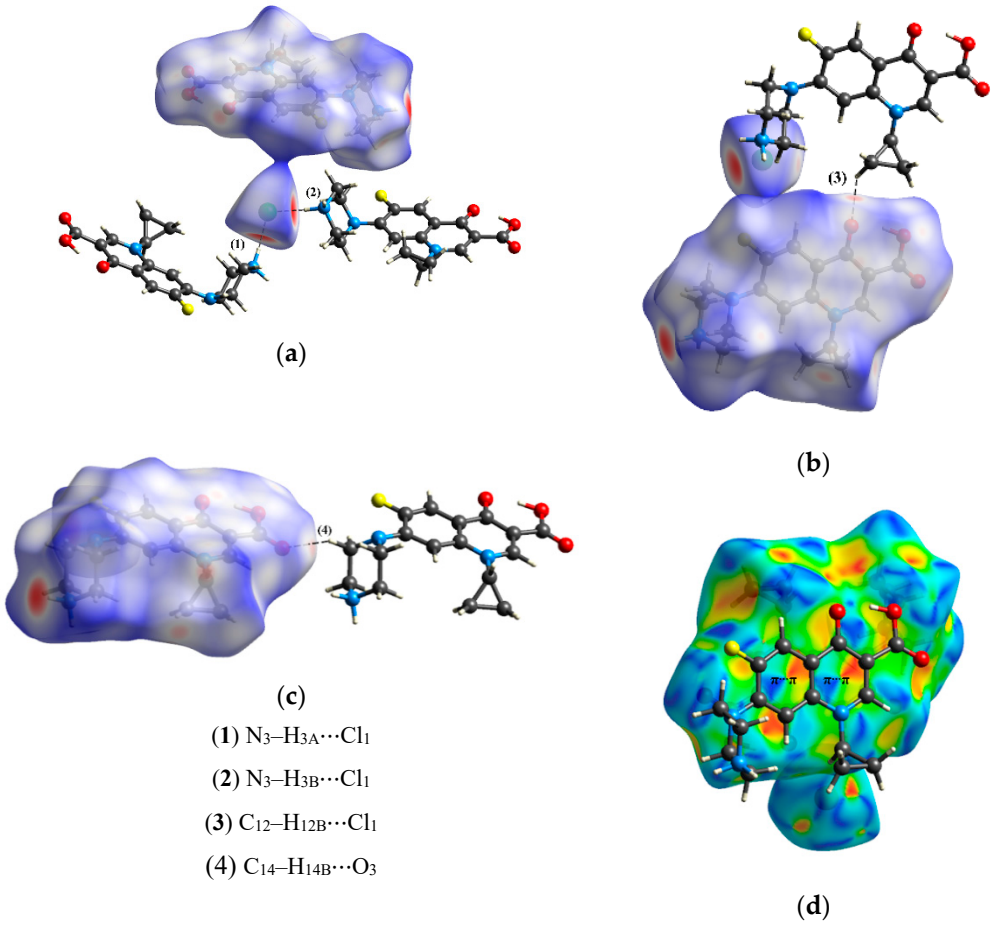

Figure 3. The HS d_{norm} showing (**a**) N_3–$H_{3A}\cdots Cl_1$ and N_3–$H_{3B}\cdots Cl_1$; (**b**) C_{12}–$H_{12A}\cdots O_1$; (**c**) C_{14}–$H_{14B}\cdots O_3$ intermolecular interactions, and (**d**) $\pi\cdots\pi$ stacking found in the crystal packing for form II of the CIP.

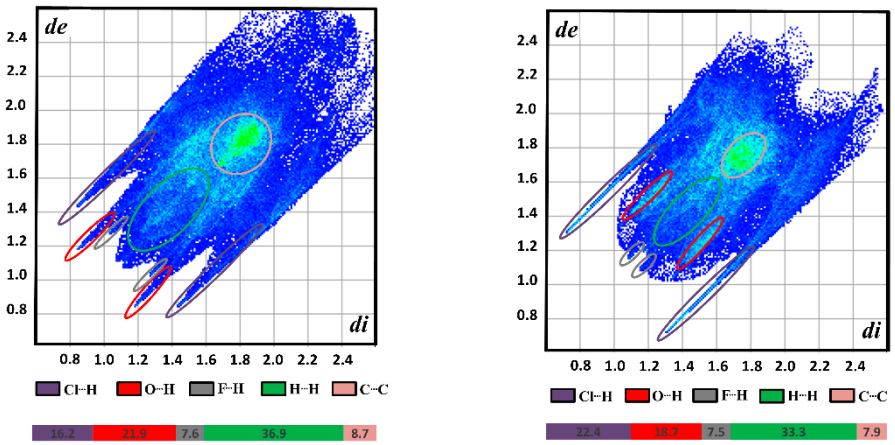

Figure 4. The representation of the 2D fingerprint plot for CIP (**a**) form I and (**b**) form II. The reciprocal contacts were included.

3.2. Molecular Modeling

Evaluation through the mean absolute percentage deviation (MAPD) indicated that the hybrid functional ωB97XD yielded the best agreement with the geometric parameters of ciprofloxacin (Supplementary Material). Specifically, this function exhibited the smallest average MAPDs for both length and bond angle (0.618%), with a difference of 0.041% between the two parameters (see Figure S1).

The frontier molecular orbital isosurfaces, HOMO and LUMO, of the CIP and ciprofloxacin hydrochloride (CIP-HCl) molecules are represented in Figure S3, and the energy values are presented in Table 2. The orbital structures are π in both molecular structures. The presence of HCl makes the compound more acidic than its neutral form, according to the HSAB principle. The HOMO energy, E_H, value in CIP is about 18.9% higher than its saline form, while the LUMO energy, E_L, value in CIP-HCL is about 17.9% lower than that in CIP. The energy gap (ΔE_{H-L}) values are also presented in Table 1 and indicate that the saline form is more stable than the neutral form. Also, the chemical hardness values indicate that CIP-HCl is a more stable form and, thus, a less polarizable compound.

Table 2. Chemical reactivity descriptors for ciprofloxacin and ciprofloxacin hydrochloride, obtained at ωB97XD/6-311++G(d,p) level of theory.

Descriptor	CIP	CIP-HCl
E_H	–139.641	–157.588
E_L	–46.881	–55.278
ΔE_{H-L}	92.759	102.310
Ionization Energy (I)	139.641	157.588
Electronic Affinity (A)	46.881	55.278
Electronegativity (χ)	93.261	106.433
Chemical potential (μ)	–93.261	–106.433
Chemical hardness (σ)	92.759	102.310
Global Electrophilicity Index (σ)	46.883	55.361

According to the global electrophilicity index values, both forms of the antibiotic drug are moderate electrophiles, with the salt form being 18.08% more electrophilic than the neutral form. The MEP maps presented in Figure S4 show the presence of a large electrophilic region in both forms of CIP. However, the electrostatic potential is more pronounced in the salt form. Furthermore, calculations of the Fukui indices showed that the C_6, C_7, and C_9 atoms of the fluoroquinolone moiety are susceptible to nucleophilic attacks in both forms of the compound. The N_2 and N_3 atoms of the heterocyclic portion can suffer electrophilic attacks in the neutral form, while in the salt form, the N_2 and O_1 atoms are susceptible to this type of attack. Finally, radical attacks can occur on O_1, C_9, and N_2 atoms in the neutral form and on O_1 and N_2 in the salt form.

The result of the TD-DFT calculations showed that the CIP-HCl system presents an absorption peak in the range of 180–350 nm of the UV-Vis spectrum, whose wavelength of maximum absorption (λ_{max}) is located at 258.2 nm, the result of a transition $\pi \rightarrow \pi^*$ (Figure 5a). This electronic transition occurs with a vertical transition energy (E) of 110.75 kcal/mol and an oscillator strength (f) of 0.7592, in which the largest contribution (76.96%) to the excited state is attributed to H–1 → L+1 excitation. In this wavelength range, electronic transitions were also observed at 289.8 nm, which occurs with an E value of 98.66 kcal/mol and a f of 0.1911, attributed to the H → L excitation, and at 242.8 nm, with an E value of 117.75 kcal/mol and a f of 0.3252, attributed to the H → L+1 excitation.

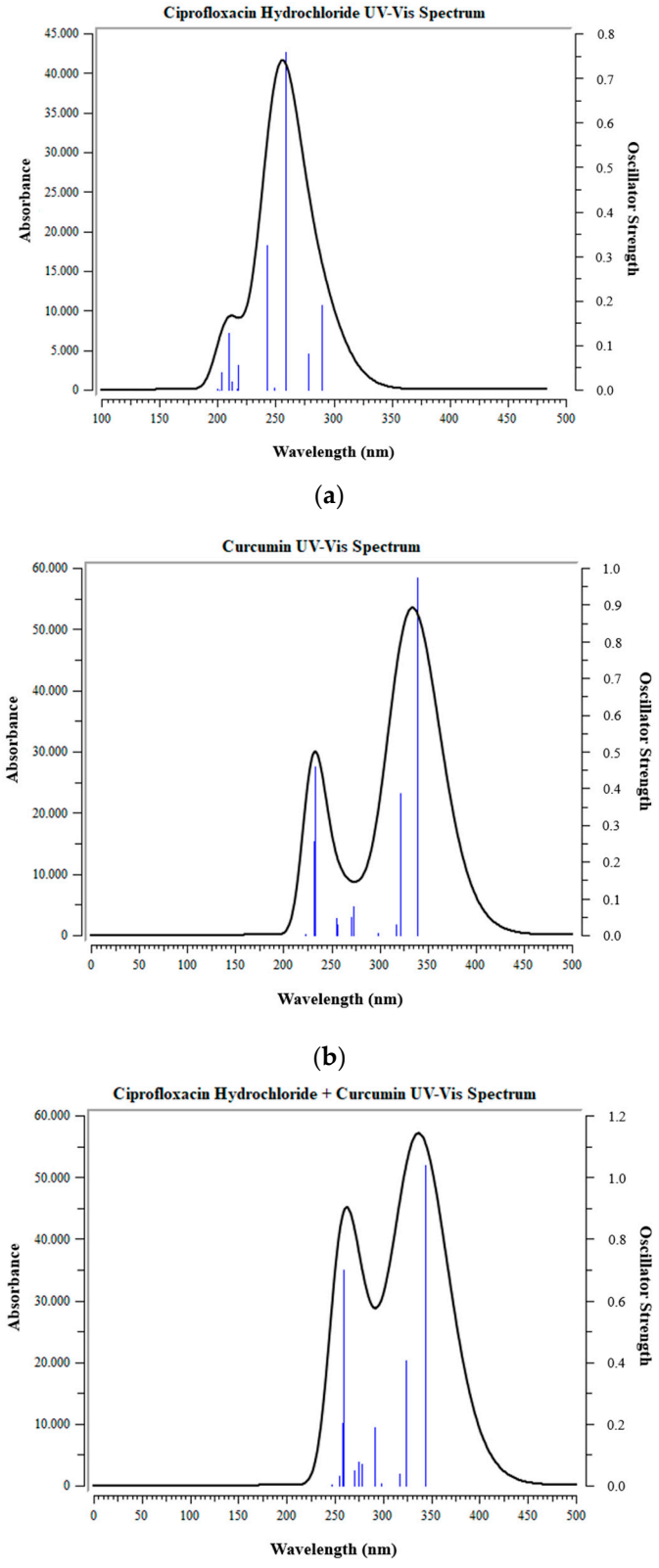

Figure 5. UV-Vis absorption spectra of (**a**) ciprofloxacin hydrochloride, (**b**) curcumin, and (**c**) CIP + CUR, obtained at TD-DFT/CAM-B3LYP/6-311++G(d,p) level of theory.

All these excitations are the result of the transition $\pi \rightarrow \pi^*$. During electronic excitation, the analysis of electron density differences between the ground and excited states [55]

revealed that electrons tend to migrate toward the regions of the carbonyl and carboxylic groups, as well as the amine group, extending to the cyclopropyl moiety. For CUR, the UV-vis absorption spectrum showed an absorption peak in the range 275–450 nm of the UV-Vis spectrum (Figure 5b), consistent with the observed experimental results. The $\pi \rightarrow \pi^*$ transition observed in the first excited state (S_1) at 339.60 nm and attributed to the H $\rightarrow$ L excitation is a result of the electronic movement of the aromatic portion towards the central region of the molecule, where the carbonyl chromophore group responsible for the photoreactive effects of CUR is present [56]. Finally, in the CIP+CUR structures, two peaks were observed: one in the range 280–475 nm and another in the range 225–280 nm (Figure 5c). The results of the calculations showed that the first peak is due to electronic excitations due to the presence of CUR, whose λ_{max} value is located around 340 nm. In this state, it was observed H $\rightarrow$ L excitation occurred at 83.107 kcal/mol with a f value of 1.0392 (like that observed for isolated CUR). The second peak has a λ_{max} value located at 259 nm which occurs from the H−3 $\rightarrow$ L+3 excitation present in the CIP molecule, at an E value roughly of 110 kcal/mol. These data indicated that CUR does not act as a protective agent for CIP in CIP+CUR complex structures.

3.3. Photodegradation Process of Ciprofloxacin Using Curcumin as Catalyst

Aiming to experimentally evaluate the photodegradation of ciprofloxacin using CUR as a catalyst and H_2O_2 as a green oxidant, the following groups were prepared: G1: 9.43 mM ciprofloxacin; G2: 9.43 mM ciprofloxacin + 1.16 M H_2O_2; G3: 9.43 mM ciprofloxacin + 4.71 mM curcumin; G4: 9.43 mM ciprofloxacin + 9.43 mM curcumin; G5: 9.43 mM ciprofloxacin + 1.16 M H_2O_2 + 4.71 mM curcumin; G6: 9.43 mM ciprofloxacin + 1.16 M hydrogen peroxide + 9.43 mM curcumin. These groups were subjected to irradiation using a light system with fluorescent lamps for time intervals of 0, 24, 48, and 72 h, respectively. The analytical evaluation and quantification of CIP were determined by HPLC. Figure 6 shows the results of the HPLC analyses in terms of CIP photodegradation percentage under the different conditions evaluated for the oxidative potential of the photocatalyst, CUR, and the oxidant, H_2O_2, respectively.

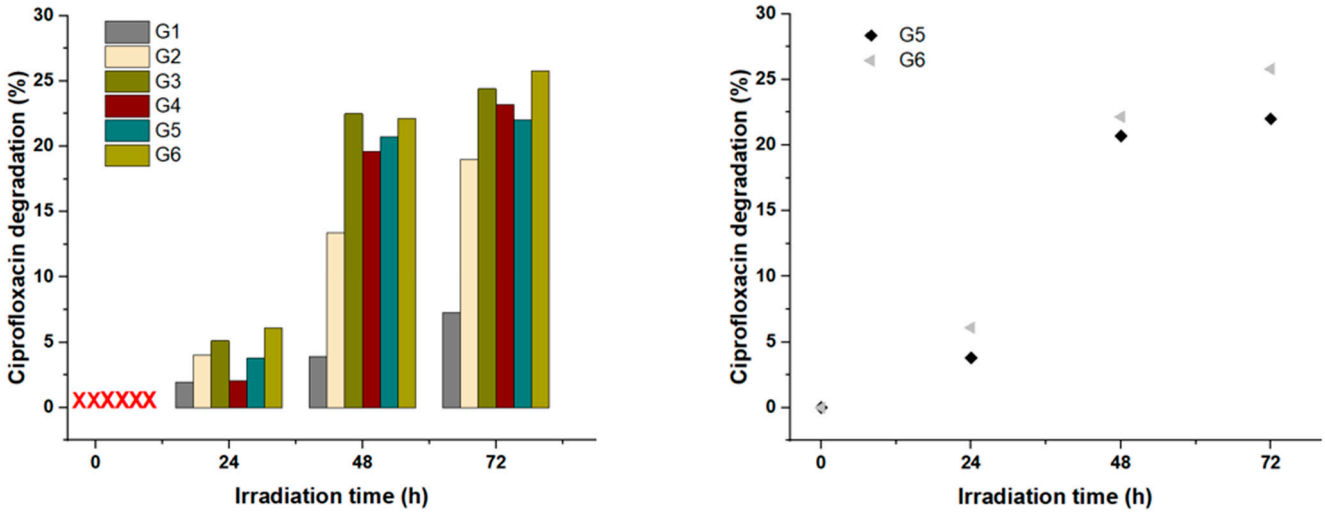

(**a**) (**b**)

Figure 6. Photodegradation data of ciprofloxacin: (**a**) **G1**: 9.43 mM ciprofloxacin; **G2**: 9.43 mM ciprofloxacin + 1.16 M H_2O_2; **G3**: 9.43 mM ciprofloxacin + 4.71 mM curcumin; **G4**: 9.43 mM ciprofloxacin + 9.43 mM curcumin; **G5**: 9.43 mM ciprofloxacin + 1.16 M H_2O_2 + 4.71 mM curcumin; **G6**: 9.43 mM ciprofloxacin + 1.16 M hydrogen peroxide + 9.43 mM curcumin; (**b**) ciprofloxacin degradation catalyzed by curcumin and hydrogen peroxide for groups (**G5** and **G6**) in function of time irradiation. The data are expressed as mean value (n = 3).

From the analysis of the data obtained and presented in Figure 6a, it was observed that CIP (**G1**) undergoes slight degradation (up to 7.3%) at the irradiation time of 72 h. When H_2O_2 was added, an increase in CIP degradation was observed (up to 19% in 72 h), which can be attributed to the direct dissociation of H_2O_2 into ·OH through absorbing ultraviolet light (<320 nm) [57]. For group **G3** (CIP + CUR (1:0.5)), a photooxidative effect was observed due to the presence of the CUR photocatalyst, resulting in a degradation of CIP of up to 24.4%. The photooxidative effect likely results from the action of photoactive CUR in the presence of O_2, generating ROS in the reaction medium [58] (Equation (1)). Furthermore, it was evaluated whether the increase in CUR concentration could result in increased degradation of CIP via photooxidative action; however, this increase in concentration (CIP + CUR (1:1)) supposedly caused competition between the CIP molecule and CUR by ROS generated in situ [59] (Equations (2)–(4)).

$$\text{Curcumin} + \text{light} \rightarrow \text{Curcumin}^* \quad (1)$$

$$\text{Curcumin}^* + {}^3O_2 \rightarrow \text{Curcumin} + \text{ROS} \quad (2)$$

$$\text{Ciprofloxacin} + \text{ROS} \rightarrow \text{Ciprofloxacin degradation products} \quad (3)$$

$$\text{Curcumin} + \text{ROS} \rightarrow \text{Curcumin degradation products} \quad (4)$$

CUR acts as a photocatalyst by absorbing light and transferring electrons or energy to O_2, generating ROS. Additionally, CUR undergoes photodegradation via a photooxidative process, leading to the formation of several photodegradation products (DP 1-9) in the presence of light and O_2 (Figure 7) [57,60]. The competition among these processes increases the rate of CUR degradation due to the oxidative action of ROS. However, this competition does not enhance the degradation of CIP, even with an increased amount of photocatalysts. Finally, the existence of a synergistic effect between the CUR photocatalyst and H_2O_2 as an oxidant in the degradation of CIP (**G5**–**G6**) was observed. However, the presence of H_2O_2 potentiated the degradation of the pharmaceutical CIP.

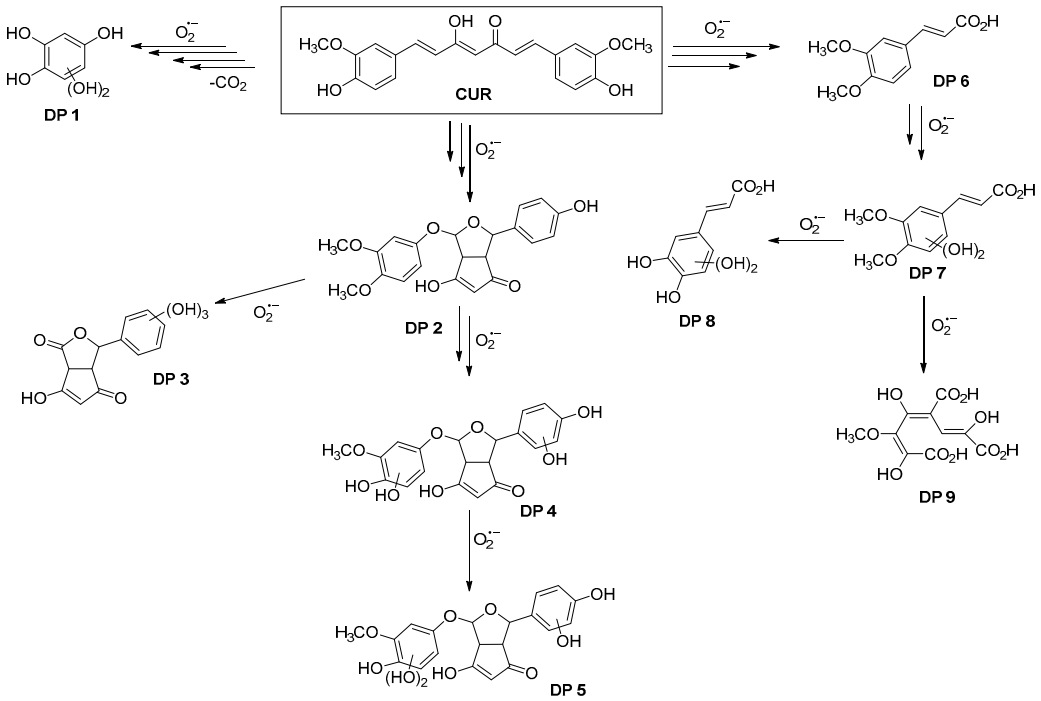

Figure 7. Proposal route for curcumin photocatalyst photodegradation in the presence of light and O_2. Adapted from Lima et al. (2022) [61].

4. Conclusions

The combination of green catalysts as oxidants can promote the photodegradation of CIP. Photocatalysis with CUR resulted in the significant degradation of CIP. However, the concentration of the CUR photocatalyst must be carefully optimized to maximize the efficiency of the photocatalytic process. Theoretical calculations indicated that the electronic excitations caused by the combined CIP + CUR structures impact the CIP drug molecule, influencing its degradation. This preliminary research demonstrated that CUR can be used as a green catalyst, and when associated with H_2O_2, it has synergistic potential in the photocatalytic degradation process, which can be applied in the environmental remediation of pharmaceutical micropollutants, whose studies are currently underway.

Supplementary Materials: The following supporting information can be downloaded at: https://www.mdpi.com/article/10.3390/separations11090260/s1, Table S1. Experimental details and refinement data of ciprofloxacin hydrochloride (CIP) polymorphic forms I and II; Table S2. Vertical excitation energies (E), absorption wavelength (λ), oscillator strength (f), and the corresponding electronic transition of the twelve excited states of ciprofloxacin hydrochloride, curcumin, and CIP + CUR complex, calculated by TD-DFT/CAM-B3LYP/6-311++G(d,p) level of theory in water; Figure S1. In (a), boxplots for the CIP geometric parameters for the B3LYP, M06-2X, wB97XD, and X3-PLYP functionals and the experimental data (XRD); in (b), the bar graphs for the mean absolute deviation percent values obtained for the CIP polymorphs I and II; and in (c), the scatter plots for the comparison of experimental and theoretical geometric parameters; Figure S2. Relaxed scan graph for the approximation of HCl and ciprofloxacin molecules; Figure S3. Frontier molecular orbitals surfaces, HOMO and LUMO, of (a) ciprofloxacin and (b) ciprofloxacin hydrochloride, obtained at the ωB97XD/6-311++G(d,p) level of theory. The orbitals were generated with an isovalue of 0.02; Figure S4. Molecular electrostatic potential at $\rho(r) = 4.0 \times 10^4$ electrons/Bohr3 contour of the total SCF electron density for (a) ciprofloxacin and (c) ciprofloxacin hydrochloride, at the ωB97XD/6-311++G(d,p) level of theory. Regions of low charge density (electrophilic) are represented by the color dark blue and regions of high charge density (nucleophilic) by the color red; Figure S5. Fukui function isosurfaces indicating the sites of (a) nucleophilic, (b) electrophilic, and (c) radical attacks generated at $\rho = 0.002$. The structures on the left correspond to the ciprofloxacin molecule and on the right, to the ciprofloxacin hydrochloride salt; Figure S6. CIP + CUR association structures optimized for excited state calculations. Interactions in (I)–(IV) structures were estimated from the nucleophilic and electrophilic regions of ciprofloxacin hydrochloride and curcumin molecules.

Author Contributions: Conceptualization, A.S.N.d.A. and L.D.D.; methodology, F.L.P.d.P., M.V.C.S., A.L.F.M., C.S.A., L.O.S., A.S.N.d.A., A.R.L., H.B.N., M.J.F.C. and L.D.D., validation, A.S.N.d.A., H.B.N., M.J.F.C. and L.D.D., formal analysis, A.R.L., H.B.N., M.J.F.C. and L.D.D., investigation, F.L.P.d.P., M.V.C.S., A.L.F.M., C.S.A., L.O.S., A.S.N.d.A., A.R.L., H.B.N., M.J.F.C. and L.D.D., resources, F.L.P.d.P., M.V.C.S., A.L.F.M., C.S.A., L.O.S., A.S.N.d.A., A.R.L., H.B.N., M.J.F.C. and L.D.D., data curation, F.L.P.d.P., M.V.C.S., A.L.F.M., C.S.A., L.O.S., A.S.N.d.A., A.R.L., H.B.N., M.J.F.C. and L.D.D., writing—original draft preparation, A.S.N.d.A., A.R.L., H.B.N., M.J.F.C. and L.D.D., writing—review and editing, A.S.N.d.A., A.R.L., H.B.N., M.J.F.C. and L.D.D., visualization, A.S.N.d.A., A.R.L., H.B.N., M.J.F.C. and L.D.D., supervision, A.S.N.d.A., A.R.L., H.B.N., M.J.F.C. and L.D.D.; project administration, L.D.D.; funding acquisition, L.D.D. All authors have read and agreed to the published version of the manuscript.

Funding: This research was funded by Fundação de Amparo à Pesquisa do Estado de Goiás (FAPEG) (201810267001556 and Inovação, Desenvolvimento e Sustentabilidade: Estreitamento entre Universidade e Setor Produtivo no Estado de Goiás Convênio para pesquisa, desenvolvimento e inovação—PD&I 07/2020, chamada pública nº 04/2023—programa de auxílio à pesquisa científica e tecnológica—aquisição de equipamentos, Chamada Pública FAPEG 12/2023 CAPES/FAPEG—Rede de pesquisa e desenvolvimento da região centro-oeste), Coordenação de Aperfeiçoamento de Pessoal de Nível Superior (CAPES) (88887.710665/2022-00, 8887.820460/2023-00). A R L acknowledges FAPESP Grant 2023/11853-6. The authors also thank Laboratório Teuto and Conselho Nacional de Pesquisa e Desenvolvimento (CNPq) (Programa Inova Talentos) for financial support.

Data Availability Statement: Data are contained within the article or Supplementary Material.

Conflicts of Interest: The authors declare no conflicts of interest.

References

1. Jia, W.-L.; Song, C.; He, L.-Y.; Wang, B.; Gao, F.-Z.; Zhang, M.; Ying, G.-G. Antibiotics in Soil and Water: Occurrence, Fate, and Risk. *Curr. Opin. Environ. Sci. Health* **2023**, *32*, 100437. [CrossRef]
2. Eyler, R.F.; Shvets, K. Clinical Pharmacology of Antibiotics. *Clin. J. Am. Soc. Nephrol.* **2019**, *14*, 1080–1090. [CrossRef] [PubMed]
3. Ruzsa, R.; Benkő, R.; Hambalek, H.; Papfalvi, E.; Csupor, D.; Nacsa, R.; Csatordai, M.; Soós, G.; Hajdú, E.; Matuz, M. Hospital Antibiotic Consumption before and during the COVID-19 Pandemic in Hungary. *Antibiotics* **2024**, *13*, 102. [CrossRef]
4. Zeng, H.; Li, J.; Zhao, W.; Xu, J.; Xu, H.; Li, D.; Zhang, J. The Current Status and Prevention of Antibiotic Pollution in Groundwater in China. *Int. J. Environ. Res. Public Health* **2022**, *19*, 11256. [CrossRef]
5. Cycoń, M.; Mrozik, A.; Piotrowska-Seget, Z. Antibiotics in the Soil Environment—Degradation and Their Impact on Microbial Activity and Diversity. *Front. Microbiol.* **2019**, *10*, 338. [CrossRef] [PubMed]
6. Tang, K.W.K.; Millar, B.C.; Moore, J.E. Antimicrobial Resistance (AMR). *Br. J. Biomed. Sci.* **2023**, *80*, 11387. [CrossRef] [PubMed]
7. Sorooshian, S. The Sustainable Development Goals of the United Nations: A Comparative Midterm Research Review. *J. Clean. Prod.* **2024**, *453*, 142272. [CrossRef]
8. Yamaguchi, N.U.; Bernardino, E.G.; Ferreira, M.E.C.; de Lima, B.P.; Pascotini, M.R.; Yamaguchi, M.U. Sustainable Development Goals: A Bibliometric Analysis of Literature Reviews. *Environ. Sci. Pollut. Res.* **2023**, *30*, 5502–5515. [CrossRef]
9. Abejew, A.A.; Wubetu, G.Y.; Fenta, T.G. Relationship between Antibiotic Consumption and Resistance: A Systematic Review. *Can. J. Infect. Dis. Med. Microbiol.* **2024**, *2024*, 9958678. [CrossRef]
10. Zay Ya, K.; Win, P.T.N.; Bielicki, J.; Lambiris, M.; Fink, G. Association Between Antimicrobial Stewardship Programs and Antibiotic Use Globally. *JAMA Netw. Open* **2023**, *6*, e2253806. [CrossRef]
11. Llor, C.; Bjerrum, L. Antimicrobial Resistance: Risk Associated with Antibiotic Overuse and Initiatives to Reduce the Problem. *Ther. Adv. Drug Saf.* **2014**, *5*, 229–241. [CrossRef] [PubMed]
12. Wang, X.; Jing, J.; Zhou, M.; Dewil, R. Recent Advances in H2O2-Based Advanced Oxidation Processes for Removal of Antibiotics from Wastewater. *Chin. Chem. Lett.* **2023**, *34*, 107621. [CrossRef]
13. Jiang, Y.; Yang, Z.; Bi, X.; Yao, N.; Zhao, P.; Meng, X. Mediated Electron Transfer Process in α-MnO2 Catalyzed Fenton-like Reaction for Oxytetracycline Degradation. *Chin. Chem. Lett.* **2024**, *35*, 109331. [CrossRef]
14. Yao, N.; Wang, X.; Yang, Z.; Zhao, P.; Meng, X. Characterization of Solid and Liquid Carbonization Products of Polyvinyl Chloride (PVC) and Investigation of the PVC-Derived Adsorbent for the Removal of Organic Compounds from Water. *J. Hazard. Mater.* **2023**, *456*, 131687. [CrossRef]
15. Bai, X.; Chen, W.; Wang, B.; Sun, T.; Wu, B.; Wang, Y. Photocatalytic Degradation of Some Typical Antibiotics: Recent Advances and Future Outlooks. *Int. J. Mol. Sci.* **2022**, *23*, 8130. [CrossRef]
16. Wu, S.; Lin, Y.; Hu, Y.H. Strategies of Tuning Catalysts for Efficient Photodegradation of Antibiotics in Water Environments: A Review. *J. Mater. Chem. A Mater.* **2021**, *9*, 2592–2611. [CrossRef]
17. Pretali, L.; Fasani, E.; Sturini, M. Current Advances on the Photocatalytic Degradation of Fluoroquinolones: Photoreaction Mechanism and Environmental Application. *Photochem. Photobiol. Sci.* **2022**, *21*, 899–912. [CrossRef]
18. Calvete, M.J.F.; Piccirillo, G.; Vinagreiro, C.S.; Pereira, M.M. Hybrid Materials for Heterogeneous Photocatalytic Degradation of Antibiotics. *Coord. Chem. Rev.* **2019**, *395*, 63–85. [CrossRef]
19. Djurišić, A.B.; He, Y.; Ng, A.M.C. Visible-Light Photocatalysts: Prospects and Challenges. *APL Mater.* **2020**, *8*, 030903. [CrossRef]
20. Gurunathan, K. Photocatalytic Hydrogen Production Using Transition Metal Ions-Doped γ-Bi2O3 Semiconductor Particles. *Int. J. Hydrogen Energy* **2004**, *29*, 933–940. [CrossRef]
21. Wang, H.; Li, J.; Huo, P.; Yan, Y.; Guan, Q. Preparation of Ag_2O/Ag_2CO_3/MWNTs Composite Photocatalysts for Enhancement of Ciprofloxacin Degradation. *Appl. Surf. Sci.* **2016**, *366*, 1–8. [CrossRef]
22. Rozmyślak, M.; Walkowiak, A.; Frankowski, M.; Wolski, L. Copper(II) Phosphate as a Promising Catalyst for the Degradation of Ciprofloxacin via Photo-Assisted Fenton-like Process. *Sci. Rep.* **2024**, *14*, 7007. [CrossRef] [PubMed]
23. Dias, I.M.; Mourão, L.C.; Andrade, L.A.; Souza, G.B.M.; Viana, J.C.V.; Oliveira, S.B.; Alonso, C.G. Degradation of Antibiotic Amoxicillin from Pharmaceutical Industry Wastewater into a Continuous Flow Reactor Using Supercritical Water Gasification. *Water Res.* **2023**, *234*, 119826. [CrossRef]
24. Piccirillo, G.; Aroso, R.T.; Rodrigues, F.M.S.; Carrilho, R.M.B.; Pinto, S.M.A.; Calvete, M.J.F.; Pereira, M.M. Oxidative Degradation of Pharmaceuticals: The Role of Tetrapyrrole-Based Catalysts. *Catalysts* **2021**, *11*, 1335. [CrossRef]
25. Piccirillo, G.; De Sousa, R.B.; Dias, L.D.; Calvete, M.J.F. Degradation of Pesticides Using Semiconducting and Tetrapyrrolic Macrocyclic Photocatalysts—A Concise Review. *Molecules* **2023**, *28*, 7677. [CrossRef] [PubMed]
26. Piccirillo, G.; Maldonado-Carmona, N.; Marques, D.L.; Villandier, N.; Calliste, C.A.; Leroy-Lhez, S.; Eusébio, M.E.S.; Calvete, M.J.F.; Pereira, M.M. Porphyrin@Lignin Nanoparticles: Reusable Photocatalysts for Effective Aqueous Degradation of Antibiotics. *Catal. Today* **2023**, *423*, 113903. [CrossRef]
27. Maldonado-Carmona, N.; Piccirillo, G.; Godard, J.; Heuzé, K.; Genin, E.; Villandier, N.; Calvete, M.J.F.; Leroy-Lhez, S. Bio-Based Matrix Photocatalysts for Photodegradation of Antibiotics. *Photochem. Photobiol. Sci.* **2024**, *23*, 587–627. [CrossRef]
28. Dias, L.D.; Blanco, K.C.; Mfouo-Tynga, I.S.; Inada, N.M.; Bagnato, V.S. Curcumin as a Photosensitizer: From Molecular Structure to Recent Advances in Antimicrobial Photodynamic Therapy. *J. Photochem. Photobiol. C Photochem. Rev.* **2020**, *45*, 100384. [CrossRef]
29. Silva, K.J.S.; Lima, A.R.; Dias, L.D.; Garbuio, M.; de Souza, M.; Correa, T.Q.; Blanco, K.C.; Sanches, E.A.; Bagnato, V.S.; Inada, N.M. Photodynamic Processes for Water and Wastewater Treatment: A Review. *Laser Phys. Lett.* **2024**, *21*, 053001. [CrossRef]

30. Rodrigues, F.M.S.; Tavares, I.; Aroso, R.T.; Dias, L.D.; Domingos, C.V.; de Faria, C.M.G.; Piccirillo, G.; Maria, T.M.R.; Carrilho, R.M.B.; Bagnato, V.S.; et al. Photoantibacterial Poly(Vinyl)Chloride Films Applying Curcumin Derivatives as Bio-Based Plasticizers and Photosensitizers. *Molecules* **2023**, *28*, 2209. [CrossRef]
31. Macrae, C.F.; Sovago, I.; Cottrell, S.J.; Galek, P.T.A.; McCabe, P.; Pidcock, E.; Platings, M.; Shields, G.P.; Stevens, J.S.; Towler, M.; et al. *Mercury 4.0*: From Visualization to Analysis, Design and Prediction. *J. Appl. Crystallogr.* **2020**, *53*, 226–235. [CrossRef] [PubMed]
32. Spackman, M.A.; Jayatilaka, D. Hirshfeld Surface Analysis. *CrystEngComm* **2009**, *11*, 19–32. [CrossRef]
33. Spek, A.L. Structure Validation in Chemical Crystallography. *Acta Crystallogr. Sect. D Biol. Crystallogr.* **2009**, *65*, 148–155. [CrossRef]
34. Spackman, P.R.; Turner, M.J.; McKinnon, J.J.; Wolff, S.K.; Grimwood, D.J.; Jayatilaka, D.; Spackman, M.A. *CrystalExplorer*: A Program for Hirshfeld Surface Analysis, Visualization and Quantitative Analysis of Molecular Crystals. *J. Appl. Crystallogr.* **2021**, *54*, 1006–1011. [CrossRef]
35. McKinnon, J.J.; Spackman, M.A.; Mitchell, A.S. Novel Tools for Visualizing and Exploring Intermolecular Interactions in Molecular Crystals. *Acta Crystallogr. Sect. B Struct. Sci.* **2004**, *60*, 627–668. [CrossRef] [PubMed]
36. Martin, A.D.; Britton, J.; Easun, T.L.; Blake, A.J.; Lewis, W.; Schröder, M. Hirshfeld Surface Investigation of Structure-Directing Interactions within Dipicolinic Acid Derivatives. *Cryst. Growth Des.* **2015**, *15*, 1697–1706. [CrossRef] [PubMed]
37. Hohenberg, P.; Kohn, W. Inhomogeneous Electron Gas. *Phys. Rev.* **1964**, *136*, B864. [CrossRef]
38. Kohn, W.; Sham, L.J. Self-Consistent Equations Including Exchange and Correlation Effects. *Phys. Rev.* **1965**, *140*, A1133–A1138. [CrossRef]
39. Frisch, M.J.; Trucks, G.W.; Schlegel, H.B.; Scuseria, G.E.; Robb, M.A.; Cheeseman, J.R.; Scalmani, G.; Barone, V.; Petersson, G.A.; Nakatsuji, H.; et al. *Gaussian 16, Revision C.01*; Gaussian, Inc.: Wallingford, CT, USA, 2016.
40. Zhao, Y.; Truhlar, D.G. The M06 Suite of Density Functionals for Main Group Thermochemistry, Thermochemical Kinetics, Noncovalent Interactions, Excited States, and Transition Elements: Two New Functionals and Systematic Testing of Four M06-Class Functionals and 12 Other Functionals. *Theor. Chem. Acc.* **2008**, *120*, 215–241. [CrossRef]
41. Becke, A.D. Density-Functional Exchange-Energy Approximation with Correct Asymptotic Behavior. *Phys. Rev. A* **1988**, *38*, 3098–3100. [CrossRef]
42. Lee, C.; Yang, W.; Parr, R.G. Development of the Colle-Salvetti Correlation-Energy Formula into a Functional of the Electron Density. *Phys. Rev. B* **1988**, *37*, 785–789. [CrossRef] [PubMed]
43. Xu, X.; Goddard, W.A. The X3LYP Extended Density Functional for Accurate Descriptions of Nonbond Interactions, Spin States, and Thermochemical Properties. *Proc. Natl. Acad. Sci. USA* **2004**, *101*, 2673–2677. [CrossRef]
44. Zhang, G.; Musgrave, C.B. Comparison of DFT Methods for Molecular Orbital Eigenvalue Calculations. *J. Phys. Chem. A* **2007**, *111*, 1554–1561. [CrossRef]
45. Zhang, J.; Lu, T. Efficient Evaluation of Electrostatic Potential with Computerized Optimized Code. *Phys. Chem. Chem. Phys.* **2021**, *23*, 20323–20328. [CrossRef] [PubMed]
46. Dennington, R.; Keith, T.A.; Millam, J.M. *GaussView 6*; Gaussian, Inc.: Wallingford, CT, USA, 2016.
47. Pearson, R.G. The Electronic Chemical Potential and Chemical Hardness. *J. Mol. Struct.* **1992**, *255*, 261–270. [CrossRef]
48. Pearson, R.G. Chemical Hardness and Density Functional Theory. *J. Chem. Sci.* **2005**, *117*, 369–377. [CrossRef]
49. Parr, R.G.; Szentpály, L.V.; Liu, S. Electrophilicity Index. *J. Am. Chem. Soc.* **1999**, *121*, 1922–1924. [CrossRef]
50. Fukui, K. Role of Frontier Orbitals in Chemical Reactions. *Science* **1982**, *218*, 747–754. [CrossRef]
51. Li, Y.; Evans, J.N.S. The Fukui Function: A Key Concept Linking Frontier Molecular Orbital Theory and the Hard-Soft-Acid-Base Principle. *J. Am. Chem. Soc.* **1995**, *117*, 7756–7759. [CrossRef]
52. Marenich, A.V.; Cramer, C.J.; Truhlar, D.G. Universal Solvation Model Based on Solute Electron Density and on a Continuum Model of the Solvent Defined by the Bulk Dielectric Constant and Atomic Surface Tensions. *J. Phys. Chem. B* **2009**, *113*, 6378–6396. [CrossRef]
53. Bauernschmitt, R.; Ahlrichs, R. Treatment of Electronic Excitations within the Adiabatic Approximation of Time Dependent Density Functional Theory. *Chem. Phys. Lett.* **1996**, *256*, 454–464. [CrossRef]
54. Bernstein, J.; Davis, R.E.; Shimoni, L.; Chang, N.-L. Patterns in Hydrogen Bonding: Functionality and Graph Set Analysis in Crystals. *Angew. Chem. Int. Ed. Engl.* **1995**, *34*, 1555–1573. [CrossRef]
55. Foresman, J.B.; Frisch, A.E. *Exploring Chemistry with Electronic Structure Methods*, 3rd ed.; Gaussian, Inc.: Wallingford, CT, USA, 2015.
56. Dias, L.D.; Aguiar, A.S.N.; de Melo, N.J.; Inada, N.M.; Borges, L.L.; de Aquino, G.L.B.; Camargo, A.J.; Bagnato, V.S.; Napolitano, H.B. Structural Basis of Antibacterial Photodynamic Action of Curcumin against S. Aureus. *Photodiagnosis Photodyn. Ther.* **2023**, *43*, 103654. [CrossRef] [PubMed]
57. Li, X.; Chen, C.; Zhao, J. Mechanism of Photodecomposition of H_2O_2 on TiO_2 Surfaces under Visible Light Irradiation. *Langmuir* **2001**, *17*, 4118–4122. [CrossRef]
58. Movaheditabar, P.; Javaherian, M.; Nobakht, V. Synthesis and Catalytic Application of a Curcumin-based Bio-MOF in One-pot Preparation of Tetrahydroquinazolinone Derivatives via Biginelli Reaction. *Appl. Organomet. Chem.* **2022**, *36*, e6602. [CrossRef]
59. Dias, L.D.; Corrêa, T.Q.; Bagnato, V.S. Cooperative and Competitive Antimicrobial Photodynamic Effects Induced by a Combination of Methylene Blue and Curcumin. *Laser Phys. Lett.* **2021**, *18*, 075601. [CrossRef]

60. Wolnicka-Glubisz, A.; Wisniewska-Becker, A. Dual Action of Curcumin as an Anti- and Pro-Oxidant from a Biophysical Perspective. *Antioxidants* **2023**, *12*, 1725. [CrossRef]
61. Lima, A.R.; Silva, C.M.; da Silva, L.M.; Machulek, A.; de Souza, A.P.; de Oliveira, K.T.; Souza, L.M.; Inada, N.M.; Bagnato, V.S.; Oliveira, S.L.; et al. Environmentally Safe Photodynamic Control of Aedes Aegypti Using Sunlight-Activated Synthetic Curcumin: Photodegradation, Aquatic Ecotoxicity, and Field Trial. *Molecules* **2022**, *27*, 5699. [CrossRef]

Disclaimer/Publisher's Note: The statements, opinions and data contained in all publications are solely those of the individual author(s) and contributor(s) and not of MDPI and/or the editor(s). MDPI and/or the editor(s) disclaim responsibility for any injury to people or property resulting from any ideas, methods, instructions or products referred to in the content.